Journal of Computational Physics 229 (2010) 4762–4780

Contents lists available at ScienceDirect

Journal of Computational Physics

journal homepage: www.elsevier.com/locate/jcp

Three-phase compressible flow in porous media: Total Differential Compatible interpolation of relative permeabilities

R. di Chiara Roupert [a,*], G. Chavent [b,c], G. Schäfer [a]

[a] Laboratoire d'Hydrologie et de Géochimie de Strasbourg, Université de Strasbourg/EOST, CNRS, 1 rue de Blessig, 67000 Strasbourg, France
[b] Inria-Rocquencourt, BP 105, 78153 Le Chesnay Cedex, France
[c] Université Paris-Dauphine, Ceremade, 75775 Paris Cedex 16, France

ARTICLE INFO

Article history:
Received 4 September 2009
Received in revised form 26 February 2010
Accepted 9 March 2010
Available online 15 March 2010

Keywords:
Multiphase flow
Porous media
Compressible flow
Global pressure
Mathematical modeling
Biharmonic equation

ABSTRACT

We describe the construction of Total Differential (TD) three-phase data for the implementation of the exact global pressure formulation for the modeling of three-phase compressible flow in porous media. This global formulation is preferred since it reduces the coupling between the pressure and saturation equations, compared to phase or weighted formulations. It simplifies the numerical analysis of the problem and boosts its computational efficiency. However, this global pressure approach exists only for three-phase data (relative permeabilities, capillary pressures) which satisfy a TD condition. Such TD three-phase data are determined by the choice of a global capillary pressure function and a global mobility function, which take both saturations and global pressure level as argument. Boundary conditions for global capillary pressure and global mobility are given such that the corresponding three-phase data are consistent with a given set of three two-phase data. The numerical construction of global capillary pressure and global mobility functions by C^1 and C^0 finite element is then performed using bi-Laplacian and Laplacian interpolation. Examples of the corresponding TD three-phase data are given for a compressible and an incompressible case.

1. Introduction

The global pressure formulation of porous flow equation was introduced for incompressible two-phase flows independently in [8,2]. It was generalized by Chavent and Jaffré [10] to compressible two- and three-phase flows under the approximation that the volume factors are evaluated at the new global pressure instead of the corresponding phase pressure. For three-phase flows, this *approached global pressure formulation* was derived under a Total Differential (TD) condition for the three-phase relative permeabilities and capillary pressures. The difficulty in obtaining physically realistic TD data [9,19] has limited the use of the global pressure in numerical simulation codes. Nevertheless, comparisons with other approaches have shown that this formulation simplifies the numerical analysis of the problem and boosts its computational efficiency [13,14].

Recently a new *exact global pressure formulation* has been developed in [1] for compressible two-phase flows, and for compressible three-phase flows in [12] under the condition that the three-phase data satisfy a *new TD condition*. In these formulations, the volume factors are evaluated at the corresponding phase pressure – and not at the global pressure as earlier.

Experimental values for three-phase relative permeabilies and capillary pressures are usually known only on the three two-phase edges of the ternary diagram $\mathbb{T}$, but rarely inside. Three-phase relative permeabilities are usually deduced from these sets of two-phase data by *interpolation formulas* such as introduced by Stone [21]. The existence of various

* Corresponding author. Tel.: +33 (0)368 850 467; fax: +33 (0)390 240 402.
E-mail address: dichiara@unistra.fr (R. di Chiara Roupert).

0021-9991/$ - see front matter © 2010 Elsevier Inc. All rights reserved.
doi:10.1016/j.jcp.2010.03.013

interpolation formulas shows that none of these formulas detains the ultimate truth. Taking advantage of this lack of experimental three-phase data, a *new class* of *TD-interpolations* was introduced by Chavent and co-workers [11,12], which allows the use of an exact global pressure formulation. The two degrees of freedom of this class are the *global capillary function* $P_c^g(s,p)$ and the *global mobility function* $d(s,p)$, where s is one saturation point in the ternary diagram and p one global pressure level.

In this new class, the number of functions which can be chosen is reduced from three (the relative permeabilities $kr_1,\ kr_2,\ kr_3$, as for example in the Stone model [21]) to two functions (the global mobility d and the global capillary pressure P_c^g). We describe in this paper the numerical implementation of one member of this TD-interpolation class, where the fractional flows and relative permeabilities are obtained by extending P_c^g and d inside the ternary diagram by means of two partial differential equations. But other choices are possible and need to be investigated.

We recall first the exact global pressure approach, with the notations and conventions introduced by Chavent and coworkers [11,12]. This leads to a simplified expression of the total volumetric flow rate, and hence to a weaker coupling between pressure and saturation equations.

Then we discuss the boundary conditions to be imposed on P_c^g and d in order to obtain TD three-phase data which coincide with the given two-phase data on the boundary $\partial\mathbb{T}$ of the ternary diagram.

Next we introduce the two finite element solvers required for the interpolation of P_c^g and d on the ternary diagram.

Finally, we show in the numerical results section TD-interpolated three-phase fractional flows and relative permeabilities obtained by this approach for two levels of compressibility.

2. Flow model

Let the fluids be numbered in order of decreasing wettability. $s_j,\ p_j$ denote the saturation and pressure levels of phase $j=1$ (water), 2 (oil) and 3 (gas), and $S_j,\ P_j$ their distribution (function of space and time variables). Ternary diagram will be denoted by $\mathbb{T}$ and its boundary by $\partial\mathbb{T}$. A three-phase saturation distribution will be denoted by $S=(S_1,S_3)$ (so that $S_2=1-S_1-S_3$), and a point of the ternary diagram by $s=(s_1,s_3)$ (so that $s_2=1-s_1-s_3$) in Fig. 1.

2.1. Conservation laws

For each phase j, one has:

$$\frac{\partial}{\partial t}(\phi(\vec{x},P_{\text{pore}})B_j(P_j)S_j)+\nabla\cdot(\varphi_j)=0,\quad j=1,2,3, \tag{1}$$

where

$\vec{x}$ = vector of spatial coordinates;
$\phi(\vec{x},P_{\text{pore}})$ = porosity;

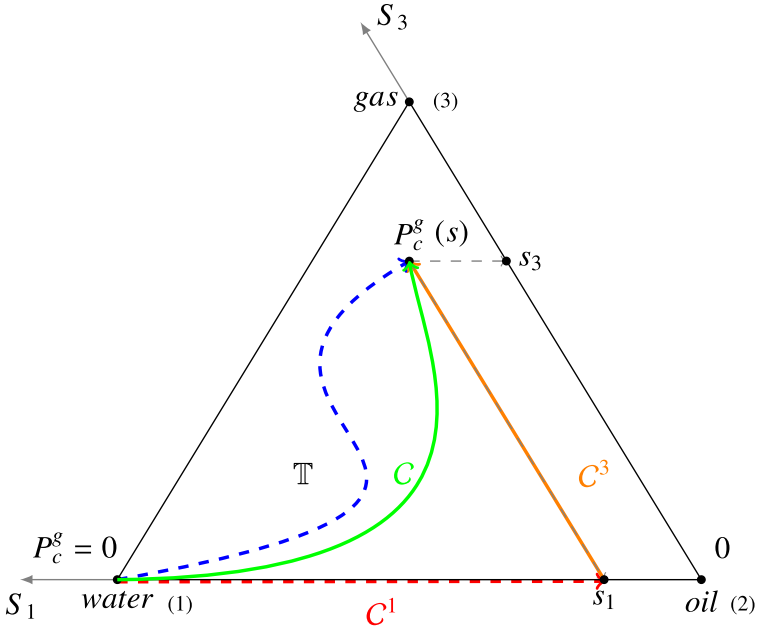

Fig. 1. Illustration of the ternary diagram $\mathbb{T}$ and different curves $\mathcal{C}$ along which $P_c^g(s,p)$ is computed.

P_{pore} = pore pressure;

and where for each phase $j = 1, 2, 3$:

$P_j(\vec{x}, t)$ = pressure;
$S_j(\vec{x}, t)$ = reduced saturation;
$\rho_j(p_j)$ = density at pressure p_j;
$\varphi_j(\vec{x}, t)$ = volumetric flow vector at pressure p_j;
$B_j(p_j) = \rho_j(p_j)/\rho_j^0$ = volume factor;

with $\sum_j S_j = 1,\ 0 \leqslant S_j \leqslant 1$ and ρ_j^0 density of phase j at reference pressure.

2.2. Muskat law

At the scale of a Representative Elementary Volume (REV) of porous medium [4], the volumetric flow vector of each phase at reference pressure for a saturation distribution $S = (S_1, S_3)$ is given by:

$$\varphi_j = -K(\vec{x}) d_j(P_j) kr_j(S)(\nabla P_j - \rho_j(P_j) g \nabla Z), \tag{2}$$

where

$K(\vec{x})$ = absolute permeability at location $\vec{x}$;
$d_j(p_j) = B_j/\mu_j$=phase mobility at pressure p_j;
$\mu_j(p_j)$ = dynamic phase viscosity at pressure p_j;
$kr_j(s)$ = relative phase permeability at saturation $s = (s_1, s_3)$;
g = gravity constant;
$Z(\vec{x})$ = depth at location $\vec{x}$.

2.3. Capillary pressure equation

The water–oil (resp. gas–oil) capillary pressures at point $\vec{x}$ is usually supposed to depend only on the water saturation (resp. the gas saturation). To ensure a positive derivative of the water–oil capillary pressure function, it is chosen opposite to the classical definition:

$$\begin{cases} P_1 - P_2 = P_c^{12}(S_1), \\ P_3 - P_2 = P_c^{32}(S_3), \end{cases} \tag{3}$$

where

$P_c^{12}(s_1)$ = water–oil capillary pressure at water saturation s_1;
$P_c^{32}(s_3)$ = gas–oil capillary pressure at gas saturation s_3.

With the chosen wettability conventions one has:

$$\begin{cases} P_c^{12}(s_1) \leqslant 0, \quad P_c^{12}(1) = 0, \quad \frac{dP_c^{12}}{ds_1}(s_1) \geqslant 0, \\ P_c^{32}(s_3) \geqslant 0, \quad P_c^{32}(0) = 0, \quad \frac{dP_c^{32}}{ds_3}(s_3) \geqslant 0. \end{cases} \tag{4}$$

2.4. Pressure equation

Classical numerical resolutions with fractional flow formulation use a " pressure equation" referring to one of the three-phase pressures, for example the oil pressure P_2, and two "saturation" equations with respect to S_1 and S_3. Summing the conservation equations in Eq. (1) for $j = 1, 2, 3$ gives

$$\frac{\partial}{\partial t}\left(\phi(\vec{x}, P_{\text{pore}}) \sum_{j=1}^{3} B_j(P_j) S_j\right) + \nabla.(\boldsymbol{q}) = 0, \tag{5}$$

where $\boldsymbol{q}$ is the *global volumetric flow* vector:

$$\boldsymbol{q} \overset{def}{=} \sum_{j=1}^{3} \varphi_j = -Kd(\nabla P_2 + f_1 \nabla P_c^{12} + f_3 \nabla P_c^{32} - \rho g \nabla Z), \tag{6}$$

where d, f_1, f_3, ρ are the global mobility, the water and gas fractional flows and the global density expressed as function of the *oil pressure level* p_2, using the capillary pressure equations in Eq. (3):

$$\begin{cases} d(s,p_2) = kr_1(s)d_1 + kr_2(s)d_2 + kr_3(s)d_3 \\ f_j(s,p_2) = kr_j(s)d_j/d(s,p_2), \quad j=1,2,3 \\ \rho(s,p_2) = \sum_{j=1}^{3} \rho_j f_j(s,p_2) \\ \sum_{j=1}^{3} f_j(s,p_2) = 1 \end{cases} \tag{7}$$

with $d_1 = d_1(p_2 + Pc^{12}(s_1))$, $d_2 = d_2(p_2)$, $d_3 = d_3(p_2 + Pc^{32}(s_3))$, and similarly for ρ_1, ρ_2, ρ_3. This "pressure equation" is strongly coupled to the saturation equations for S_1 and S_3 by the two gradient-of-capillary-pressure terms in the right-hand side of Eq. (6).

2.5. Definition of global pressure field and global capillary pressure function

To find a more suitable form for the pressure equation, a new "global pressure" field P [10,12] is introduced, with the objective that:

- the gradient-of-capillary-pressure coupling terms are eliminated from the formula for the global volumetric flow:

$$\boldsymbol{q} \approx -Kd[\nabla P - \rho g \nabla Z]. \tag{8}$$

Hence P and $\boldsymbol{q}$ will follow a Darcy-like law, so one can expect that P exhibits a smooth behaviour

- P is in the range of the phase pressures:

$$P_{\min} \leqslant P_1 \leqslant P \leqslant P_3 \leqslant P_{\max}. \tag{9}$$

This will allow to use the global pressure P as pore pressure P_{pore} in the case of pressure dependent porosities.

Therefore, a comparison of $\boldsymbol{q}$ in Eqs. (6) and (8) suggests to require that the global pressure field P is related to the oil pressure and saturation fields P_2 and $S = (S_1, S_3)$ by:

$$P = P_2 + P_c^g(S,P), \tag{10}$$

where P_c^g is a *global capillary pressure* function, to be determined. In order to achieve the objectives on P, this function has to satisfy first:

$$\begin{cases} \forall (S_1(\vec{x},t), S_2(\vec{x},t), S_3(\vec{x},t), P(\vec{x},t)), \\ \nabla P_c^g(S,P) = f_1(S,P)\nabla P_c^{12}(S_1) + f_3(S,P)\nabla P_c^{32}(S_3) + \frac{\partial p}{\partial p}(S,P)\nabla P. \end{cases} \tag{11}$$

where ∇ denotes the gradient with respect to the space variable $\vec{x}$. When this condition is satisfied, the volumetric flow rate becomes:

$$\boldsymbol{q} = -Kd\left[\left(1 - \frac{\partial P_c^g}{\partial p}\right)\nabla P - \rho g \nabla Z\right], \tag{12}$$

so that Eq. (8) is essentially satisfied. If moreover P_c^g is chosen such that:

$$P_c^g = 0 \quad \text{for } s = (1,0), \text{ which correspond to the water summit of } \mathbb{T}, \tag{13}$$

then condition (9) is also satisfied (see Eq. (17) below).

The global pressure field P is uniquely determined by Eq. (10) once the oil pressure and saturation fields P_2 and $S = (S_1, S_3)$ are known, provided P_c^g satisfies the *stability condition* [10,12]:

$$\forall s \in \mathbb{T}, \quad p_{\min} \leqslant p \leqslant p_{\max}, \quad \left|\frac{\partial P_c^g}{\partial p}(s,p)\right| < 1. \tag{14}$$

We call "compressibility factor" the quantity $\partial P_c^g/\partial p$. It has to remain small if the desired formulation is to exist.

3. Existence of a global pressure formulation

A global pressure formulation will exist as soon as one can find a *global capillary pressure* function $(s,p) \rightsquigarrow P_c^g$ that satisfies conditions given by Eqs. (11), (13) and (14). But it is always possible to satisfy Eq. (13) once (11) and (14) hold, as these latter involve only derivatives of P_c^g. So we focus on conditions which ensure that (11) and (14) can be satisfied. The global pressure level $p \in [p_{\min}, p_{\max}]$ is fixed throughout this section.

3.1. Satisfying (11): Total differential condition

Condition formulated in Eq. (11) is equivalent to:

$$\forall s \in \mathbb{T} \text{ one has : } \begin{cases} \frac{\partial P_c^g}{\partial s_1}(s,p) = f_1(s, p - P_c^g)\frac{dP_c^{12}}{ds_1}(s_1), \\ \frac{\partial P_c^g}{\partial s_3}(s,p) = f_3(s, p - P_c^g)\frac{dP_c^{32}}{ds_3}(s_3). \end{cases} \tag{15}$$

This implies that P_c^g satisfies a differential equation along any given smooth curve $\mathcal{C} : t \in [0,1] \rightsquigarrow (\mathcal{C}_1(t), \mathcal{C}_3(t)) \in \mathbb{T}$ of the ternary diagram. Of particular interest are the curves $\mathcal{C}$ starting at $(s_1, s_3) = (1, 0)$ (water, where $P_c^g = 0$) and ending at a given point $s = (s_1, s_3)$ of $\mathbb{T}$ (see Fig. 1). Along such a curve, the function $\beta(t) = P_c^g(\mathcal{C}(t), p)$ satisfies:

$$\begin{cases} \frac{d\beta}{dt} = f_1(\mathcal{C}, p - \beta)\frac{dP_c^{12}}{ds_1}\mathcal{C}_1' + f_3(\mathcal{C}, p - \beta)\frac{dP_c^{32}}{ds_3}\mathcal{C}_3', \quad \beta(0) = 0, \\ \beta(1) = P_{cg}(s_1, s_3, p) \text{ independently of the curve } \mathcal{C}, \end{cases} \tag{16}$$

where $\mathcal{C}_j' = d\mathcal{C}_j/dt$. The independency condition stated in Eq. (16) is the *Total Differential (TD) condition* which has to be satisfied by the fractional flows $f_1,\ f_3$ and the capillary pressure functions $P_c^{12},\ P_c^{32}$ in order to ensure the existence of P_c^g, and hence of the global pressure P.

When this condition is satisfied, the value of P_c^g at a given point (s_1, s_3) of $\mathbb{T}$ and a given global pressure level p can be expressed for example by integration along the curve made of $\mathcal{C}^1 = (1 - t + ts_1, 0)$ followed by $\mathcal{C}^3 = (0, ts_3)$ (see Fig. 1). But here $\mathcal{C}_1^{1\prime} = -1 + s_1,\ \mathcal{C}_3^{1\prime} = 0$ and $\mathcal{C}_1^{3\prime} = 0,\ \mathcal{C}_3^{3\prime} = s_3$, which gives:

$$\begin{cases} \frac{d\beta^1}{dt} = -f_1(\mathcal{C}^1, p - \beta^1)\frac{dP_c^{12}}{ds_1}(\mathcal{C}_1^1)(1 - s_1), \quad \beta^1(0) = 0 \\ \frac{d\beta^3}{dt} = f_3(\mathcal{C}^3, p - \beta^3)\frac{dP_c^{32}}{ds_3}(\mathcal{C}_3^3)s_3, \quad \beta^3(0) = \beta^1(1) \\ P_c^g(s_1, s_3, p) = \beta^3(1) \end{cases} \tag{17}$$

where β^1 and β^3 are expression of β along $\mathcal{C}^1$ and $\mathcal{C}^3$ curves. This formula is useful for the mathematical analysis of the new formulation (see for example the next section). However it cannot be used for the numerical determination of P_c^g for a given set of three-phase fractional flows and capillary pressures, as there is no simple way to know wether this set satisfies the TD condition given by Eq. (16) or not – and in general it will not!

3.2. Satisfying the stability condition given by Eq. (14)

Let us compute the compressibility factor $\partial P_c^g/\partial p(s,p)$ at a given point $s = (s_1, s_3) \in \mathbb{T}$. Following [12], we introduce $\gamma^j(t) \stackrel{\text{def}}{=} \partial P_c^g/\partial p(\mathcal{C}^j(t), p)$ for $j = 1, 3$, and derive the previous system of Eq. (17) with respect to p, which leads to:

$$\begin{cases} \frac{d\gamma^1}{dt} = -\frac{\partial f_1}{\partial p_2}(\mathcal{C}^1, p - \beta^1)\frac{dP_c^{12}}{ds_1}(\mathcal{C}_1^1)(1 - s_1)(1 - \gamma^1), \quad \gamma^1(0) = 0, \\ \frac{d\gamma^3}{dt} = \frac{\partial f_3}{\partial p_2}(\mathcal{C}^3, p - \beta^3)\frac{dP_c^{32}}{ds_3}(\mathcal{C}_3^3)s_3(1 - \gamma^3), \quad \gamma^3(0) = \gamma^1(1), \\ \frac{\partial P_c^g}{\partial p}(s_1, s_3, p) = \gamma^3(1). \end{cases} \tag{18}$$

The two first lines of Eq. (18) are differential equations of the form:

$$\frac{d\gamma^j}{dt} = \underbrace{\frac{\partial f_j}{\partial p_2}(\mathcal{C}^j, p - \beta^j)\frac{dP_c^{j2}}{ds_j}(\mathcal{C}_j^j)\mathcal{C}_j^{j\prime}}_{\stackrel{\text{def}}{=} \alpha^j(t)}(1 - \gamma^j), \quad \gamma^j(0) = \gamma_0^j, \tag{19}$$

whose analytical solution is given by:

$$\gamma^j(t) = 1 - (1 - \gamma_0^j)\exp\left(-\int_0^t \alpha^j(\tau)d\tau\right). \tag{20}$$

Using (20) and initial values of (18), the third line of (18) is then given by:

$$\begin{aligned} \frac{\partial P_c^g}{\partial p}(s,p) &= 1 - (1 - \gamma^1(1))\exp\left(-\int_0^1 \alpha^3(\tau)d\tau\right) \\ &= 1 - \exp\left(-\int_0^1 \left[\alpha^1(\tau) + \alpha^3(\tau)\right]d\tau\right). \end{aligned} \tag{21}$$

This shows that the coefficient $1 - \partial P_c^g/\partial p$, required for the implementation of the global pressure formulation (see Eq. (12)) is strictly positive, and gives a simple way to compute it - and of course to check wether the stability condition (14) is satisfied or not for the problem at hand ! We refer to [12] for conditions on the mobilities $d_j,\ j = 1, 2, 3$ under which (14) hold true.

3.3. Remark on a single compressible phase case (gas)

When the compressibility of water and oil are neglected, the derivatives of phase mobilities are zero with respect to their own phase pressure ($d_1' = d_2' = 0$). Therefore $\partial f_1/\partial p_2 = 0$ and hence $\alpha^1 = 0$. Then a simple calculation shows that:

$$\alpha^3(\tau) = \frac{kr_3 d_3'(kr_1 d_1 + kr_2 d_2)}{(kr_1 d_1 + kr_2 d_2 + kr_3 d_3)^2} \frac{\mathrm{d}P_c^{32}}{\mathrm{d}s_3}(\tau s_3) s_3 \geqslant 0,$$

where $\tau \in [0,1]$. Three-phase relative permeabilities $kr_1,\ kr_2,\ kr_3$ are evaluated at $(\tau s_1, \tau s_3)$ and $d_1,\ d_2,\ d_3,\ d_3'$ are computed at the corresponding phase pressure. It leads to:

$$\frac{\partial P_c^g}{\partial p}(s_1, 0, p) = 0 \quad \text{on the water—oil side,}$$
$$0 \leqslant \frac{\partial P_c^g}{\partial p}(s_1, s_3, p) < 1 \quad \text{over } \mathbb{T}.$$

In particular, the stability condition formulated in expression (14) is automatically satisfied. In the numerical examples presented below, maximum values of $\partial P_c^g/\partial p$ are in the order of 10^{-4}, so that $1 - \partial P_c^g/\partial p \simeq 1$.

4. A Partial Differential Equation-Total Differential (PDE-TD) interpolation algorithm for two-phase data

In order to take advantage of the exact global pressure formulation recalled in the previous sections, it is necessary to be able to construct secondary flow variables such as three-phase relative permeabilities and capillary pressures, which both coincide with given two-phase data on the side of the ternary diagram AND satisfy the TD condition (16). We present in this section one such algorithm (adapted from [12]), which uses partial differential equations to extend d and P_c^g over the ternary diagram, as well as the two-phase data sets to which it will be applied. Let p be a given global pressure level in the range of interest.

4.1. The PDE-TD-interpolation algorithm

The PDE-TD-interpolation algorithm needs as input a collection of three two-phase relative permeabilities curves $kr_i^{ij},\ kr_j^{ij}$, two capillary pressure curves $P_c^{12},\ P_c^{32}$, the viscosities μ_i of each fluid, plus the gas compressibility data (see algorithm). Note that water and oil are supposed to be incompressible ($B_1 = B_2 = 1$).

PDE-TD-interpolation algorithm

Require: p, kr_k^{ij} for $k = i, j$, $P_c^{12}(s_1)$, $P_c^{32}(s_3)$ for all s_1, s_3 in [0,1], $M_3,\ R,\ T_3,\ \rho_3^0,\ \mu_i$

Ensure: $kr_i(s,p),\ v_i(s,p),\ \partial P_c^g/\partial p(s,p)$ for all s in $\mathbb{T}$

***step* 1:** Solve non-linear Ordinary Differential Equations to obtain $(P_c^g)^{data}$ on $\partial\mathbb{T}$

***step* 2:** Correct two-phase data for TD Compatibility

***step* 3:** Compute d on $\partial\mathbb{T}$

***step* 4:** Solve harmonic problem

$$\begin{cases} -\Delta d = 0 & in\ \mathbb{T} \\ d = d^{data} & in\ \partial\mathbb{T} \end{cases}$$

***step* 5:** Solve biharmonic problem

$$\begin{cases} \Delta^2 P_c^g = 0 & in\ \mathbb{T} \\ P_c^g = (P_c^g)^{data} & on\ \partial\mathbb{T} \\ \frac{\partial P_c^g}{\partial \boldsymbol{n}} = \left(\frac{\partial P_c^g}{\partial \boldsymbol{n}}\right)^{data} & on\ \partial\mathbb{T}_{13},\ \partial\mathbb{T}_{23} \text{ and } \partial\mathbb{T}_{12} \end{cases} \rightarrow \text{Compute } v_i,\ d_i$$

***step* 6:** Compute $\frac{\partial P_c^g}{\partial p}(s,p),\ kr_i(s,p)$

We solve first in step 1 *Initial Value Problems* Eq. (16) on two-phase side(s) of $\mathbb{T}$ with an *Ordinary Differential Equation (ODE) Solver*: starting at the water summit (1,0), where $P_c^g = 0$, one determines $(P_c^g)^{data} \stackrel{\text{def}}{=} \beta$ on the rest of the boundary. Solving for example one ODE on the water–gas side, and the other on the water–oil resp. oil–gas sides will produce in general two different values of $\beta = (P_c^g)^{data}$ at the gas summit (0,1), which violates the TD condition Eq. (16).

So we correct in step 2 the two-phase data in order to satisfy the TD condition Eq. (16) on $\partial\mathbb{T}$: one modifies $(P_c^g)^{data}$ on the gas–oil side for example in such a way that it matches at the gas vertex the value of $(P_c^g)^{data}$ computed on the water–gas side. This might modify slightly the relative permeabilitiy data on the gas–oil side.

Then we compute in step 3 the global mobility d^{data} on $\partial\mathbb{T}$ *at the given global pressure level p*, which is given by Eq. (7) with P_2 replaced by $P - P_c^g(s,p)$. In step 4, the global mobility d is then extended to the interior of $\mathbb{T}$ by solving an harmonic equation on $\mathbb{T}$ by mean of C^0 piecewise linear finite elements.

Step 5 is devoted to the extension of the global capillary pressure $(P_c^g)^{data}$ to the inside of $\mathbb{T}$. In order to ensure that the fractional flows associated to P_c^g by Eq. (15) coincide on $\partial\mathbb{T}$ with those derived from the data, it is necessary for P_c^g to satisfy both the Dirichlet condition $P_c^g = (P_c^g)^{data}$ and a Neumann condition on $\partial\mathbb{T}$. Hence P_c^g will be extended to $\mathbb{T}$ as the solution of a biharmonic equation which satisfies these Dirichlet and Neumann conditions. This equation is solved by a C^1 *Hsieh–Clough–Tocher* finite element method [16], which ensure that the fractional flows derived from P_c^g are continuous over the ternary diagram. For each fluid phase, the corresponding fractional flow and phase mobility are then derived.

Finally, the TD relative permeabilities are computed from P_c^g and d and the stability condition is verified. The different steps introduced in the PDE-TD-interpolation algorithm are discussed in the following sections.

4.2. The two-phase data sets

Data usually available for the engineer in environmental sciences or in reservoir modeling are three sets of two-phase data on capillary pressure and relative permeabilities for water–gas, gas–oil and water–oil system. Two global pressure levels p are studied: in case one, $p = 1$ bar, and the gas volume factor B_3 remains close to one over $\mathbb{T}$ (nearly incompressible flow); in case two, $p = 1.2$ bar, so that B_3 is near to 1.15 (compressible flow). Conventions for diagram $\mathbb{T}$ are given in Fig. 1, and the three edges of $\mathbb{T}$ are parameterized by the three curves:

$$\begin{cases} \mathcal{C}^{12}(t) = (1-t,0), \\ \mathcal{C}^{23}(t) = (0,t), \\ \mathcal{C}^{13}(t) = (1-t,t), \end{cases} \qquad \forall t \in [0,1]. \tag{22}$$

The ternary diagram is discretized with triangles equally spaced in S_1 and S_3 directions following $\Delta s_1 = \Delta s_3 = 0.1$.

The data set is then made of

- the single phase characteristics, as given in Table 1 for cases 1 and 2,
- the capillary pressure functions $P_c^{32}(s_3)$ and $P_c^{12}(s_1)$ defined on $\mathbb{T}$, with the chosen wettability convention, as shown in Fig. 3,
- the relative phase permeabilities $kr_k^{ij}(t)$ at point $C^{ij}(t)$ of $\partial\mathbb{T}$, for $k = i$ or j and $ij = 12$, 23 and 13, as shown in Fig. 2.

The input to the interpolation algorithm will then be:

- the derivatives of the capillary pressure curves: $P_c^{k2\prime} = \mathrm{d}P_c^{k2}/\mathrm{d}s_k$ *for* $k = 1,3$,
- the fractional flow $f_k^{ij}(t,p_2)$ of fluid k and the total mobility $d^{ij}(t,p_2)$ at point $C^{ij}(t)$

of each edge ij for a given oil pressure level p_2. They are easily computed from the data using formula (7).

5. Determination of $P_c^g(s,p)$ on ∂T (step 1)

Determination of $P_c^g(s,p)$ on $\partial\mathbb{T}$ requires to solve three non-linear Ordinary Differential Equations (ODE's) along three curves $\mathcal{C}$ of $\mathbb{T}$ defined in (22). We shall use the notations following notations for quantities which depend on the global pressure:

$$\beta^{ij}(t) = P_c^g(\mathcal{C}^{ij}(t),p),$$
$$v_k^{ij}(t,p) = f_k^{ij}(t,p-\beta^{ij}(t)) \quad \textit{for } k = i,j \text{ and } ij = 12,23 \text{ and } 13.$$

Table 1
Initial single phase data settings on $\partial\mathbb{T}$ for cases 1 and 2.

Property	Symbol	Value	Unit
Water dynamic viscosity	μ_1	1	$\times 10^{-3}$ [Pa s]
Oil dynamic viscosity	μ_2	0.5	$\times 10^{-3}$ [Pa s]
Gas dynamic viscosity	μ_3	0.015	$\times 10^{-3}$ [Pa s]
Molar mass of gas phase	M_3	0.025	[kg mol^{-1}]
Temperature of gas phase	T_3	296	[K]
Ideal gas law constant	R	8.314	[J K^1 mol^1]
Reference gas density at 1 bar	ρ_3^0	1.204	[kg m^{-3}]
Water and oil volume factor	B_1, B_2	1	[–]

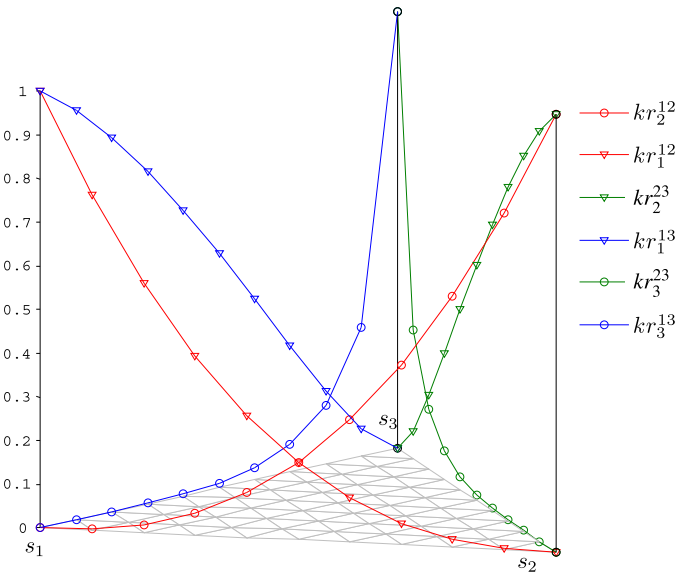

Fig. 2. Initial relative two-phase permeabilities given on $\partial\mathbb{T}_{12}$, $\partial\mathbb{T}_{13}$ and $\partial\mathbb{T}_{23}$ for cases 1 and 2.

5.1. Determination of β^{12} along the water–oil side $\partial\mathbb{T}_{12}$

We solve the ODE system starting from $\beta^{12}(0) = P_c^g(C^{12}(0), p) = P_c^g(1, 0, p) = 0$ to the ending point at $s_1 = 0$ (i.e. $s_2 = 1$):

$$\begin{cases} \beta^{12}(0) = 0, \\ \frac{d\beta^{12}}{dt}(t) = -f_1^{12}(t, p - \beta^{12}(t)) P_c^{12\prime}(1-t), \end{cases} \tag{23}$$

The water is supposed incompressible, so that $B_1 = 1$ and the *water–oil* ODE system is simply reduced to:

$$\begin{cases} \beta^{12}(0) = 0, \\ \frac{d\beta^{12}}{dt}(t) = -\frac{kr_1^{12}(t)}{\mu_1 d^{12}(t)} P_c^{12\prime}(1-t). \end{cases} \tag{24}$$

5.2. Determination of β^{23} along the gas–oil side $\partial\mathbb{T}_{23}$

The initial condition for β^{23} at $s_3 = 0$ (or $s_2 = 1$) is obtained from the final value $\beta^{12}(1)$ of β^{12} on the *water–oil* side:

$$\begin{cases} \beta^{23}(0) = \beta^{12}(1), \\ \frac{d\beta^{23}}{dt}(t) = f_3^{23}(t, p - \beta^{23}(t)) P_c^{32\prime}(t), \end{cases} \tag{25}$$

Thus the *gas–oil* ODE system can be expressed by:

$$\begin{cases} \beta^{23}(0) = \beta^{12}(1), \\ \frac{d\beta^{23}}{dt}(t) = kr_3^{23}(t) \frac{d_3(p - \beta^{23}(t) + P_c^{32}(t))}{d^{23}(t, p - \beta^{23}(t))} P_c^{32\prime}(t). \end{cases} \tag{26}$$

5.3. Determination of β^{13} along the water–gas side $\partial\mathbb{T}_{13}$

Based on the conditions formulated in Section 3, the first initial value is given by the global capillary pressure at $s_1 = 1$ i.e. $\beta^{13}(0) = \beta^{12}(0) = 0$

$$\begin{cases} \beta^{13}(0) = 0, \\ \frac{d\beta^{13}}{dt}(t) = -f_1^{13}(t, p - \beta^{13}(t)) P_c^{12\prime}(1-t) + f_3^{13}(t, p - \beta^{13}(t)) P_c^{32\prime}(t). \end{cases} \tag{27}$$

Thus the *water–gas* ODE system can be expressed by:

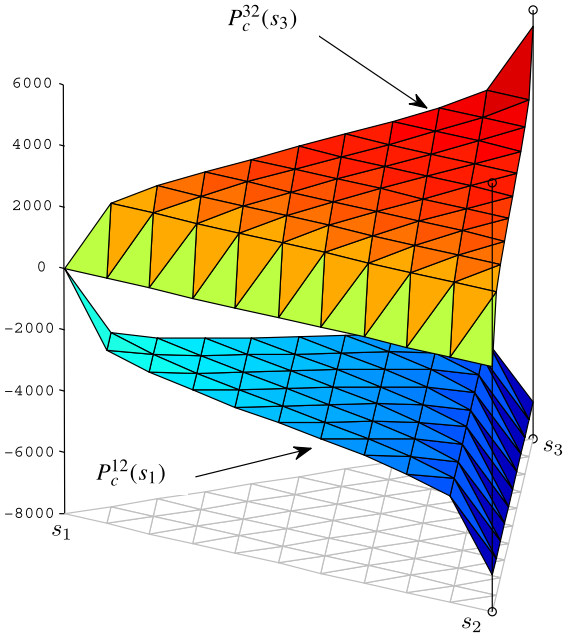

Fig. 3. Capillary pressure P_c^{32} [Pa] (top) and P_c^{12} [Pa] (bottom) given on $\mathbb{T}$ for cases 1 and 2.

$$\begin{cases} \beta^{13}(0) = 0, \\ \frac{d\beta^{13}}{dt}(t) = -\frac{kr_1^{13}(t)P_c^{12\prime}(1-t)}{\mu_1 d^{13}(t,p-\beta^{13}(t))} + \frac{kr_3^{13}(t)d_3(p-\beta^{13}(t)+P_c^{32}(t))P_c^{32\prime}(t)}{d^{13}(t,p-\beta^{13}(t))}. \end{cases} \tag{28}$$

In order to solve the given three ODE's system, we used a multistep predictor–corrector scheme.

5.4. Computing $\beta = P_c^g$ on $\partial\mathbb{T}$ with a predictor–corrector scheme $P(EC)_\mu^m E$

Let β_k^{ij} denotes the global capillary pressure computed on side (ij) at node t_k. A multistep predictor–corrector is used to compute $\beta = P_c^g$ on $\partial\mathbb{T}$. Practically, only initial point (t_0, β_0^{ij}) is used to compute (t_1, β_1^{ij}), and in general, β_k^{ij} is needed to compute β_{k+1}^{ij}. After several points found, it is feasible to use several prior points in the calculation. In our case, we used an Adams four-step method [20] to solve ODE's system on $\partial\mathbb{T}_{12}$ (23), on $\partial\mathbb{T}_{23}$ (25) and on $\partial\mathbb{T}_{13}$ (27). It requires β_{k-3}^{ij}, β_{k-2}^{ij}, β_{k-1}^{ij}, and β_k^{ij} in the calculation of β_{k+1}^{ij}. The chosen method is not self-starting ; four initial points (t_0, β_0^{ij}), (t_1, β_1^{ij}), (t_2, β_2^{ij}), and (t_3, β_3^{ij}), must be given in advance in order to generate the points $[(t_k, \beta_k^{ij}) : k \geqslant 4]$. We used a fourth-order Runge–Kutta scheme. A desirable feature of the multistep scheme is the determination of the local truncation error (LTE). Hence, a correction term is added, which improves the accuracy of the solution at each step. A grid parameter μ is used to determine how many times each step is divided and controls that for each refined step, the *local truncature error* (LTE) is reached and β_{k+1}^{ij} converges after m linearized loops. Using combinations of a predictor (P) and corrector (C), one requires only two function evaluations (E) of the right-hand side per step. Basically, predictor–corrector methods proceed by extrapolating of a polynomial fit (Adams–Bashforth scheme) to the derivative from the previous points to the new point (the predictor step) and then use it to interpolate (Adams–Moulton scheme) the derivative in the corrector step to take into account gas pressure at each step. Each ODE system is built up from its first *initial* value. Numerical results are shown for cases 1 and 2 in Figs. 4 and 7, respectively. In general, the ODE for β^{23} gives a value at $s_3 = 1$ which is slightly different from the one obtained on water–gas side for β^{13}. In order to satisfy the TDC condition, a correction is applied to close the boundary system on $\partial\mathbb{T}$ (see Fig. 3). This will be discussed in details in Section 6.

6. Satisfying the *Total Differential Compatibility* condition (step 2)

The global capillary function P_c^g, when it exists, take a unique value at the gas vertex. It is hence necessary that β^{23} and β^{13} satisfy the *TD Compatibility condition* [12].

$$\beta^{23}(1) = \beta^{13}(1). \tag{29}$$

Based on Eqs. (23), (25) and (27), an integral expression of the global capillary pressure at $s_3 = 1$ is obtained using two different paths (see Fig. 1):

- from $s_1 = 1$ to $s_1 = 0$ along the water–oil side $(\mathcal{C}^1)$ and from $s_3 = 0$ to $s_3 = 1$ along the gas–oil side $(\mathcal{C}^3)$;
- from $s_1 = 1$ to $s_3 = 1$ along the water–gas side

$$\int_0^1 \left[v_1^{12}(\tau,p) - v_1^{13}(\tau,p)\right] P_c^{12\prime}(1-\tau)\mathrm{d}\tau = \int_0^1 \left[v_3^{32}(\tau,p) - v_3^{13}(\tau,p)\right] P_c^{32\prime}(\tau)\mathrm{d}\tau. \tag{30}$$

This shows that for example the simple fractional flow model which satisfies $v_1^{12} = v_1^{13}$ and $v_3^{32} = v_3^{13}$, respects the TDC condition. But in general, the functions β^{23} and β^{13} computed from the data will not satisfy exactly the TDC condition (29). So we enforce this condition by modifying slightly one of the beta functions, for example β^{23}:

$$\beta_{TD}^{23}(t) = \beta^{23}(t) - t^2(\beta^{23}(1) - \beta^{13}(1)). \tag{31}$$

An illustration of the corrected values β_{TD}^{23} is given below in Fig. 3. For each global pressure level p, this correction leads to a new permeability model $kr_{2,TD}^{23}$ and $kr_{3,TD}^{23}$ on the gas–oil side which is quite similar to the initial one. Once corrected for TDC condition, the functions β^{12}, β^{23} and β^{13} give a Dirichlet condition for P_c^g. Some rules must be checked to ensure a correct calculation of the solution. Using Eqs. (4), (15) and (27), one can see that:

$$\begin{aligned}
&\beta^{13}(t) = \int_0^t \frac{\partial P_c^g}{\partial s_3}(1-t,\tau,p)\mathrm{d}\tau + \beta^{12}(t),\\
&\beta^{13}(t) - \beta^{12}(t) = \int_0^t \underbrace{f_3(1-t,\tau,p_2)}_{0\leqslant\cdot\leqslant 1}\underbrace{\frac{\mathrm{d}P_c^{32}}{\mathrm{d}s_3}(\tau)}_{\geqslant 0}\mathrm{d}\tau,\\
&\Rightarrow |\beta^{13}(t) - \beta^{12}(t)| \leqslant \underbrace{P_c^{32}(t)}_{\geqslant 0} - \underbrace{P_c^{32}(0)}_{=0},\\
&\Longleftrightarrow \beta^{13}(t) - P_c^{32}(t) \leqslant \beta^{12}(t) \leqslant \beta^{13}(t).
\end{aligned} \tag{32}$$

We get a similar relation for $\beta^{23}(t)$ on gas–oil side $\partial\mathbb{T}_{23}$. Hence a necessary condition for the fractional flows f_1 and f_3 associated to the function P_c^g under determination to range between 0 and 1 is:

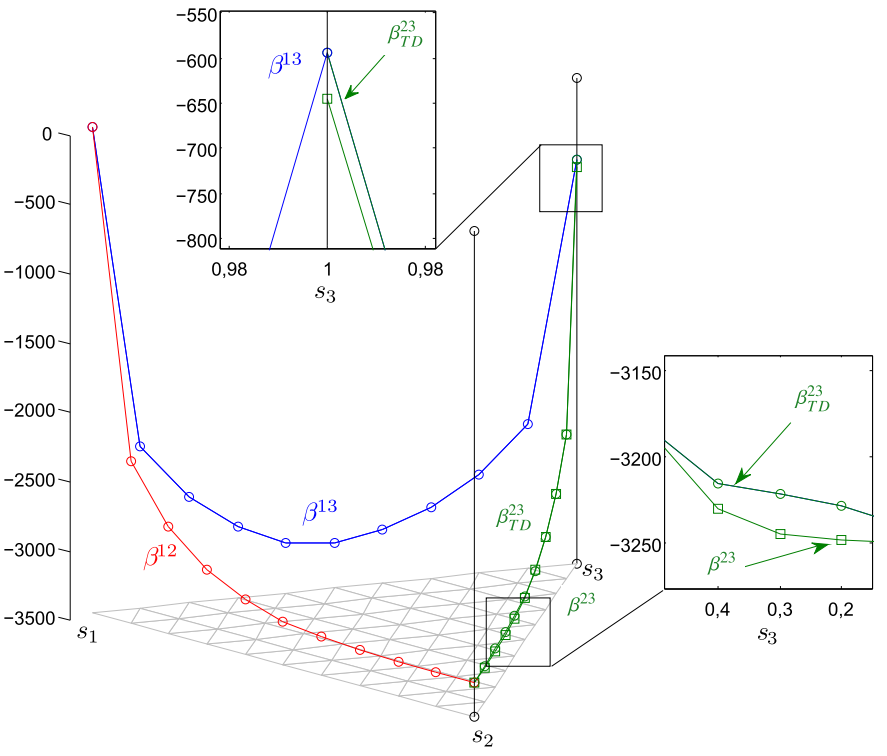

Fig. 4. Numerical results for β^{ij} [Pa] over $\partial\mathbb{T}$ using $P(EC)_{10}^2E$, case 1.

$$\begin{cases} \beta^{13}(t) - (P_c^{12}(1-t) - P_c^{12}(0)) \leqslant \beta_{TD}^{23}(t) \leqslant \beta^{13}(t), \\ \beta^{13}(t) - P_c^{32}(t) \leqslant \beta^{12}(t) \leqslant \beta^{13}(t). \end{cases} \tag{33}$$

Right-hand side of these two inequalities are respected for both β_{TD}^{23} and β^{12} (see Fig. 4) and ensure that fractional flows will vary from zero to one.

7. Determination of $\boldsymbol{d}(\boldsymbol{s},\boldsymbol{p})$ on $\partial\boldsymbol{T}$ and $\boldsymbol{T}$ (steps 3 and 4)

7.1. Dirichlet boundary condition on $d(s,p)$ over $\partial\mathbb{T}$ (step 3)

The global capillary pressure is known on $\partial\mathbb{T}$ (Sections 5 and 6). It is hence possible to compute the value d^{data} of the global mobility associated to the data at the given global pressure level p

$$d^{data} = \begin{cases} d^{12} = kr_1^{12} d_1 + kr_2^{12} d_2 & \text{(water—oil)}, \\ d^{13} = kr_1^{13} d_1 + kr_3^{13} d_3 (p - \beta^{13} + P_c^{32}) & \text{(water—gas)}, \\ d^{23} = kr_2^{23} d_2 + kr_3^{23} d_3 (p - \beta_{TD}^{23} + P_c^{32}) & \text{(gas—oil)}. \end{cases} \tag{34}$$

This function will serve as Dirichlet boundary condition for the determination of d over $\mathbb{T}$. Values of d^{12}, d^{23} and d^{13} are shown as part of the complete solution over $\mathbb{T}$ in Figs. 5 and 6.

7.2. C^0 finite element for Laplace problem on $d(s,p)$ over $\mathbb{T}$ (step 4)

In this TD-interpolation algorithm, d is chosen as the smoothest function which interpolates the boundary conditions d^{data}, by solving an harmonic problem. This problem is solved by standard finite elements C^0. The resulting global mobility is presented for case 1 and case 2 in Figs. 5 and 6, respectively. The red-doted line is the value of d^{12} on water–oil side, the green one stands for d^{23} on gas–oil side and the blue d^{13} for water–gas side.

8. Determination of $\boldsymbol{P_c^g}(\boldsymbol{s},\boldsymbol{p})$ on $\boldsymbol{T}$ (step 5)

In order to obtain fractional flow functions which are continuous over $\mathbb{T}$, it is necessary (see Eq. (15)) to represent P_c^g by a piecewise polynomial where both the function and the derivatives meet at the boundary between elements. Those finite elements are called H^2 – *conforming finite elements*, and therefore can be used for the approximation of the fourth-order problem of step 5 [7,6]. For triangular finite elements, there exist two popular families of polynomial spaces. *Argyris* finite element [3]

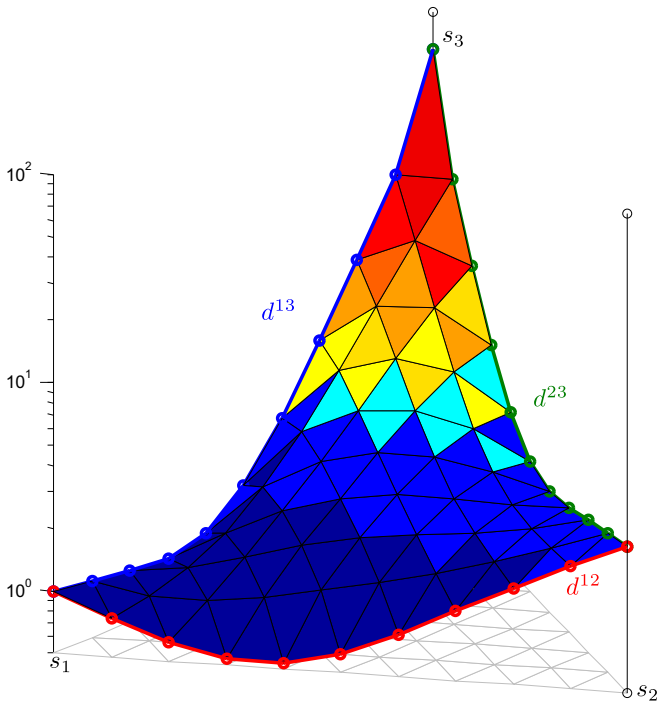

Fig. 5. Global mobility solution d of the Laplace problem, case 1.

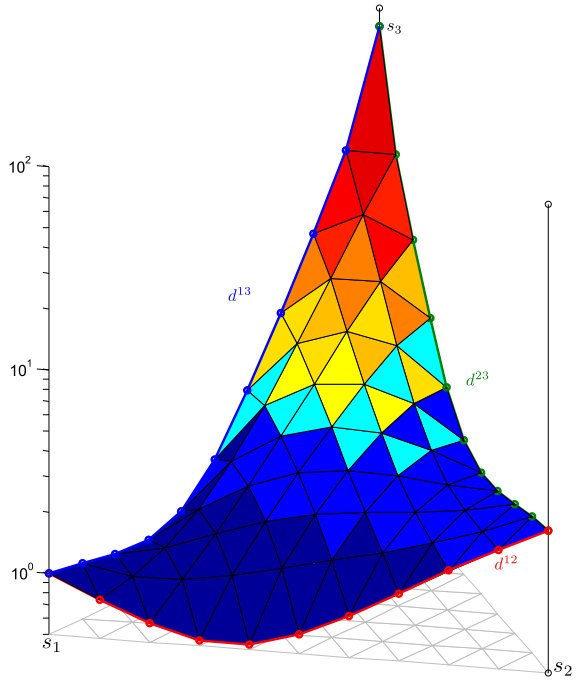

Fig. 6. Global mobility solution d of the Laplace problem, case 2.

uses complete quintic polynomial expansion with five degrees of freedom on each vertex (its value, first and second derivatives) and one on the middle of each side (normal derivatives). Deleting the normal mid-nodes, one have *Bell* triangular finite elements [5].

The high approximation qualities of these elements are well known but need some regularity for data and solution to solve fourth-order problems. Therefore we use another popular family of C^1 triangular finite element called the *complete Hsieh–Clough–Tocher* (HCT) finite element described by [6,7,16].

In the HCT finite element approach, an elementary triangle is subdivided in three subtriangles using the center of gravity [5]. This element has three degrees of freedom at each node located at a vertex of the triangle (value of the function and of its two derivatives), plus the normal derivatives at the mid-side nodes. The choice of the interior node as barycenter does not influence the solution [15]. On each subtriangles, a complete cubic polynomial expansion is used. The resulting function is C^1-class on the assembled element. System solved in step 5 is similar to the problem solved in the case of the deflexion of a thin elastic plate, *clamped* at its boundaries with a zero loading.

8.1. Boundary condition over $\partial\mathbb{T}$

The value of P_c^g at a node s of $\partial\mathbb{T}_{ij}$ is using the results of step 1:

$$\left(P_c^g(s)\right)^{data} = \beta^{ij}(t) \quad \text{where } t \text{ is such that } \mathcal{C}^{ij}(t) = s. \tag{35}$$

Then the derivatives $\partial P_c^g/\partial s_1$ and $\partial P_c^g/\partial s_3$ at the same node s are given, using Eq. (15), by:

$$\left(\frac{\partial P_c^g}{\partial s_j}(s)\right)^{data} = f_j(s, p - (P_c^g)^{data}) P_c^{j2'}(s_j) \quad \text{for } j = 1, 3. \tag{36}$$

So we require in our interpolation code that the global capillary pressure P_c^g satisfies:

- at each node s of $\partial\mathbb{T}$ which is a vertex of an element:

$$P_c^g(s) = \left(P_c^g(s)\right)^{data}, \tag{37}$$

$$\frac{\partial P_c^g}{\partial s_j}(s) = \left(\frac{\partial P_c^g}{\partial s_j}(s)\right)^{data} \quad \text{for } j = 1, 3. \tag{38}$$

- at each node s of $\partial\mathbb{T}$ which is the middle of an edge:

$$\left(\frac{\partial P_c^g}{\partial \boldsymbol{n}}(s)\right) = \left(\frac{\partial P_c^g}{\partial \boldsymbol{n}}(s)\right)^{data}, \tag{39}$$

where the normal derivative $\left(\frac{\partial P_c^g}{\partial \boldsymbol{n}}(s)\right)^{data}$ is computed by combination of $\left(\frac{\partial P_c^g}{\partial s_1}(s)\right)^{data}$ and $\left(\frac{\partial P_c^g}{\partial s_3}(s)\right)^{data}$.

In order to interpret these conditions, one notices that conditions in Eq. (38) are equivalent to:

$$\left(\frac{\partial P_c^g}{\partial t}(s)\right) = \left(\frac{\partial P_c^g}{\partial t}(s)\right)^{data}, \tag{40}$$

$$\left(\frac{\partial P_c^g}{\partial \boldsymbol{n}}(s)\right) = \left(\frac{\partial P_c^g}{\partial \boldsymbol{n}}(s)\right)^{data}, \tag{41}$$

where the tangential derivative $\left(\frac{\partial P_c^g}{\partial t}(s)\right)^{data}$ is computed by combination of $\left(\frac{\partial P_c^g}{\partial s_1}(s)\right)^{data}$ and $\left(\frac{\partial P_c^g}{\partial s_3}(s)\right)^{data}$.

Conditions in Eqs. (37) and (40) at vertex nodes constrain the value of P_c^g on $\partial\mathbb{T}$: they constitute a Dirichlet condition ; conditions in Eq. (39) at mid-edge nodes and (41) at vertex nodes, which constrain the normal derivative of P_c^g, constitute a Neumann condition.

8.2. Solving the biharmonic problem for $P_c^g(s,p)$ using C^1 finite elements

The biharmonic problem of step 5 is solved using the HCT finite elements at the given global pressure level $P_{\min} \leqslant p \leqslant P_{\max}$. It produces, at each node s of $\mathbb{T}$, a value of the global capillary pressure $P_c^g(s,p)$ and two derivatives $\partial P_c^g/\partial s_1(s,p)$ and $\partial P_c^g/\partial s_3(s,p)$.

We have plotted in Figs. 7–9 resp. the functions $P_c^g = p - p_2$, $P_c^g - P_c^{12} = p - p_1$ and $P_c^g - P_c^{32} = p - p_3$, which give the relation of the global pressure p with each individual phase pressure over the ternary diagram. One sees that for each phase j, the relation between p and p_j is smooth near the jth vertex of $\mathbb{T}$, i.e. where the jth phase represents the main part of the flow and the jth phase pressure distribution P_j is expected to vary smoothly over the flow domain. Hence the global pressure distribution P is expected to be smooth all over the flow domain. On the contrary, in the classical formulation where the numerical unknown is the oil pressure (for example), the variation of $p_2 - p_1 = P_c^{21}$ and $p_2 - p_3 = P_c^{32}$ with saturation is given by the

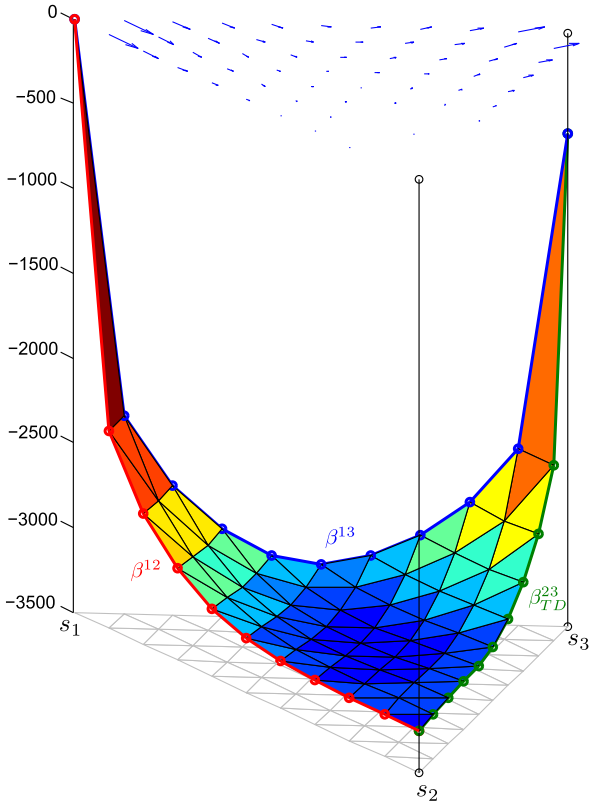

Fig. 7. Numerical results for β^{ij} [Pa] over $\partial\mathbb{T}$ using $P(EC)^2_{10}E$ from step 1, global capillary pressure $p - p_2 = P_c^g(s,p)$ and $(\partial P_c^g/\partial s_1;\ \partial P_c^g/\partial s_3)$ (blue arrows) computed from step 5, case 2. (For interpretation of the references in colour in this figure legend, the reader is referred to the web version of this article.)

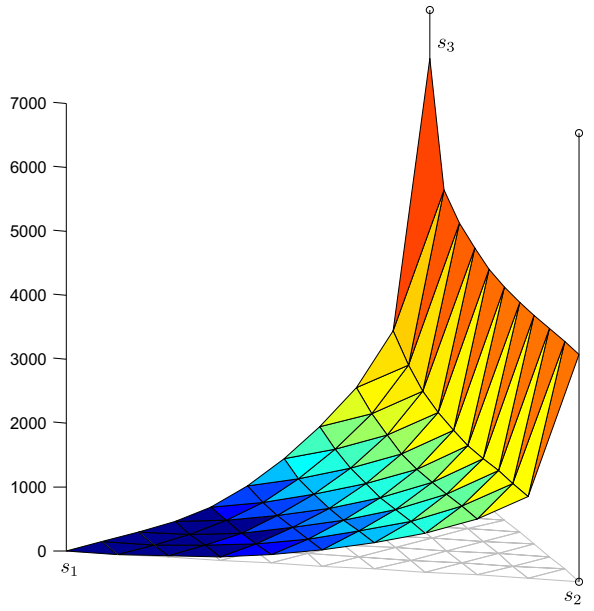

Fig. 8. Relation of global pressure to water pressure: $p - p_1 = P_c^g(s,p) - P_c^{12}(s_1)$, case 2.

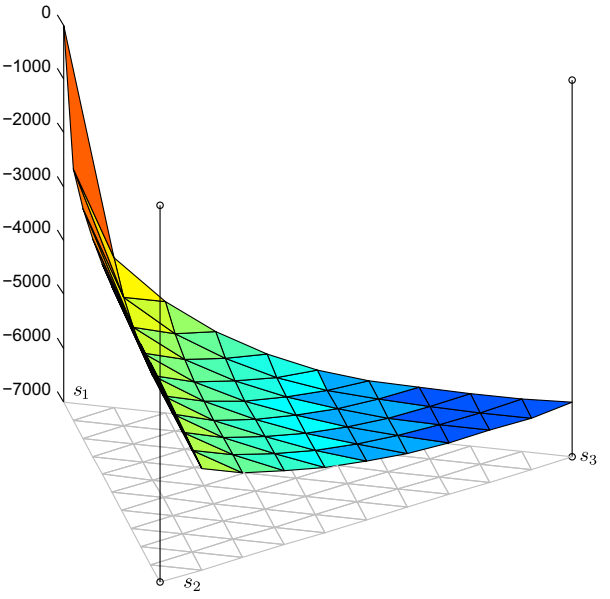

Fig. 9. Relation of global pressure to gas pressure: $p - p_3 = P_c^g(s,p) - P_c^{32}(s_3)$, case 2.

capillary pressure functions of Fig. 3, where it is seen that $p_2 - p_j$ is singular near the jth vertex for $j = 1,3$: the oil pressure distribution P_2 is expected to exhibit steep variations at flow locations where the saturations are close to the water or gas vertex. This shows the global pressure is a smoother unknown then the oil pressure, and is hence best fitted for numerical approximation.

As one can see on Figs. 7–9, conditions (33) are verified for both cases 1 and 2. Once P_c^g has been determined, the associated fractional flow $v_i(s,p)$ with $i = 1,2,3$ are defined by:

$$\begin{cases} v_1(s,p) = \left(\frac{\partial P_c^g}{\partial s_1}(s,p)\right)\left(\frac{dP_c^{12}}{ds_1}(s_1)\right)^{-1}, \\ v_3(s,p) = \left(\frac{\partial P_c^g}{\partial s_3}(s,p)\right)\left(\frac{dP_c^{32}}{ds_3}(s_3)\right)^{-1}, \\ v_2(s,p) = 1 - v_1(s,p) - v_3(s,p). \end{cases} \tag{42}$$

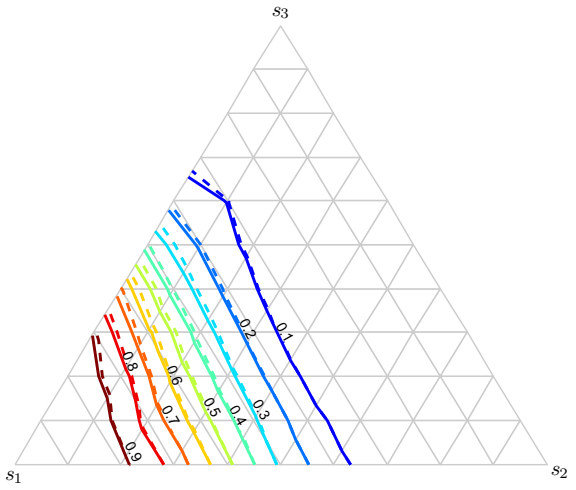

Fig. 10. Water fractional flow $v_1(s,p)$ for case 1 (dashed line) and case 2 (solid line) on $\mathbb{T}$.

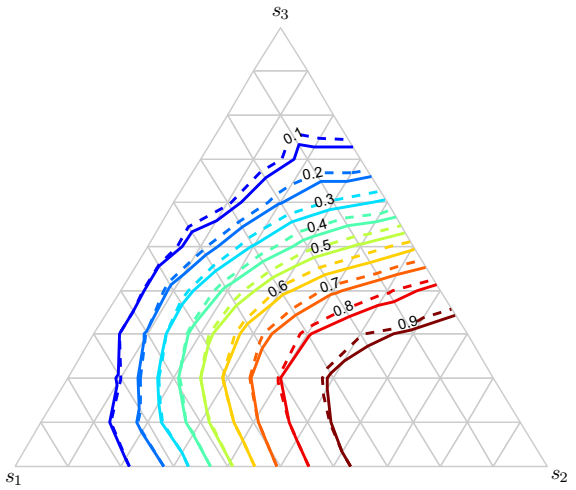

Fig. 11. Oil fractional flow $v_2(s,p)$ for case 1 (dashed line) and case 2 (solid line) on $\mathbb{T}$.

By construction, these fractional flow satisfy the TD condition (15).

Figs. 10–12 show the resulting phase fractional flow obtained in cases 1 and 2. One can see that the water fractional flow v_1 and oil fractional flow v_2 are the same on the water–oil sidein both case due to their respective volume factors $B_1 = B_2 = 1$ (see Figs. 10 and 11). However, the compressibility effect is visible on the two gas/liquid sides i.e. the gas–oil edge and the water–gas edge in Fig. 12: remember that the gas mobility d_3 is computed using the gas volume factor B_3 evaluated at the gas pressure.

Note that the global algebraic system is symmetric, while local bending stiffness HCT matrix is unsymmetric. These two linear systems are respectively solved by an iterative preconditioned conjugate gradient (PCG) solver and a direct solver based on both unifrontal/multifrontal methods well suited for solving sparse linear systems (UMFPACK) [17]. The Eisenstat trick [18] is applied to the preconditioned matrix (PCG) and allows saving a significant part of computation. Integrals are computed with a 12-order Hammer–Gauss quadrature.

9. Determination of kr_1, kr_2, kr_3 and $\partial P_c^g/\partial p$ on T (step 6)

Figs. 13–15 show the three-phase relative permeabilities $kr_i(s,p)$ deduced from the fractional flow $v_i(s,p)$ from step 5, the global mobility $d(s,p)$ from step 4 and the individual phase mobility d_i by the formulas:

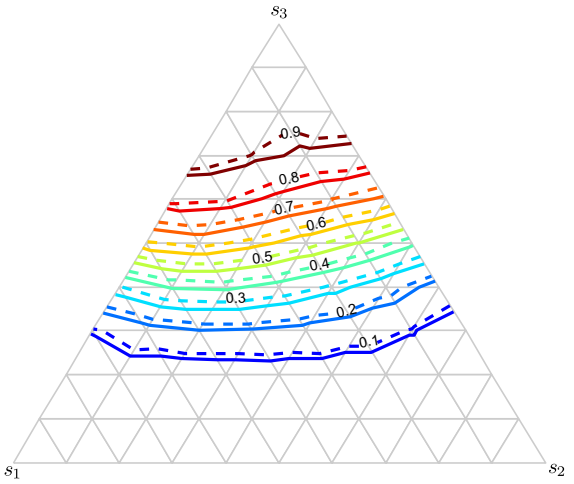

Fig. 12. Gas fractional flow $v_3(s,p)$ for case 1 (dashed line) and case 2 (solid line) on $\mathbb{T}$.

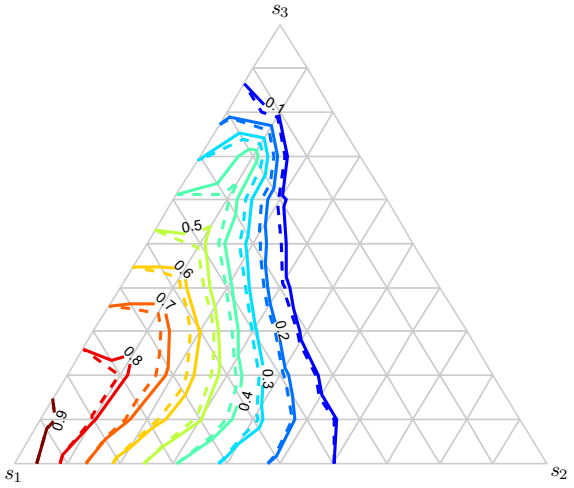

Fig. 13. Relative permeability of water $kr_1(s,p)$ for case 1 (dashed line) and case 2 (solid line) on $\mathbb{T}$.

$$\begin{cases} kr_1(s,p) = \frac{v_1(s,p)}{d_1}\, d(s,p), \\ kr_2(s,p) = \frac{v_2(s,p)}{d_2}\, d(s,p), \\ kr_3(s,p) = \frac{v_3(s,p)}{d_3(p - P_c^g(s,p) + P_c^{32}(s_3))}\, d(s,p). \end{cases} \tag{43}$$

By construction, these relative permeabilities coincide with the two phase data on the boundary $\partial\mathbb{T}$. To discuss differences between cases 1 and 2, relative error $|kr_i - kr_i^*|/kr_i$ (* stand for case 1), $i = 1,2,3$ is calculated at $s_1 = 10\%,\ s_3 = 40\%$. At this point, water relative permeability of case 2 is 15% higher than incompressible case 1 and relative permeabilities of the gas resp. oil phase are 5% higher and 7% lower in case 2, respectively. Hence, with the interpolation scheme used by the algorithm, the gas compressibility allows water to achieve higher water relative permeabilities at higher gas saturations.

An expression of the compressibility factor $\partial P_c^g/\partial p$ appearing in formula (12) for the global volumetric flow can be derived from Eq. (21) in the case of a single compressible phase:

$$\frac{\partial P_c^g}{\partial p}(s,p) = 1 - \exp\left(- \int_0^1 \underbrace{\frac{kr_3 d_3'(kr_1 d_1 + kr_2 d_2)}{(kr_1 d_1 + kr_2 d_2 + kr_3 d_3)^2} P_c'^{32} s_3}_{\alpha^3(\tau)}\, \mathrm{d}\tau \right). \tag{44}$$

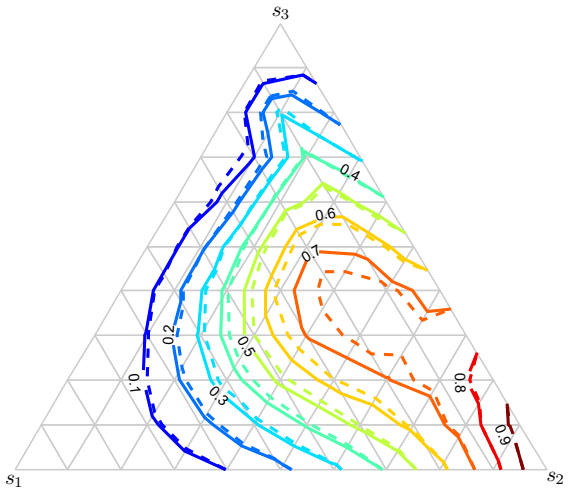

Fig. 14. Relative permeability of oil $kr_2(s,p)$ for case 1 (dashed line) and case 2 (solid line) on $\mathbb{T}$.

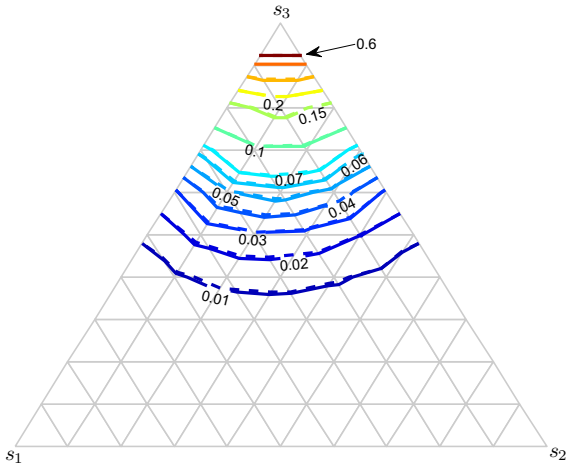

Fig. 15. Relative permeability of gas $kr_3(s,p)$ for case 1 (dashed line) and case 2 (solid line) on $\mathbb{T}$.

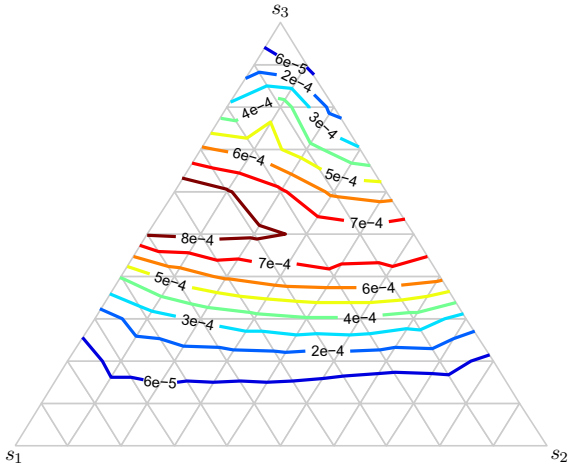

Fig. 16. Compressibility factor $\partial p_c^g/\partial p$ for case 2.

With a convenient Simpson integration rule, one gets for each interior node (s_1, s_3) of $\mathbb{T}$:

$$\frac{\partial P_c^g}{\partial p}(s,p) \simeq 1 - \exp\left(-\frac{\alpha^3(1)}{2}\right), \tag{45}$$

with here $\alpha^3(0) = \partial f_3/\partial p_2(C^3(0), p - \beta^3(0)) = 0$. The compressibility factor $\partial P_c^g/\partial p$ obtained on $\mathbb{T}$ for case 2 is shown in Fig. 16. The maximum value calculated is about 10^{-3}. Numerical results show that it vanishes at the water, oil and gas vertex, and that it remains small compared to one over the ternary diagram. Of course, for case 1, $d_3' = 0$ and hence $\partial P_c^g/\partial p = 0$. On the water–gas system, the compressibility factor is significantly higher than the one determined on the oil–gas side. However, on the water–oil side, the compressibility factor is zero due to $B_1 = B_2 = 1$.

10. Conclusion

We develop in this paper, a new Partial Differential Equation-Total Differential (PDE-TD) interpolation algorithm for the determination of three-phase flow in the case of a single compressible phase (gas). This algorithm takes as input a classical collection of two-phase data, and corrects slightly the two-phase relative permeabilities for TD condition This might have little impact on the resolution at the reservoir scale, as it is well known that the shock saturation mainly dominates two-phase flows, but ensures the existence of a global capillary pressure $P_c^g(s,p)$, from which the three-phase fractional flows and relative permeabilities are derived. By construction, these relative permeabilities satisfy the TD condition, and allow to replace the classical compressible flow formulation by the fully equivalent global pressure formulation [12], where the global pressure is defined by $P = P_2 + P_c^g(S,P)$. The algorithm involves the resolution of an harmonic and a biharmonic problem over the ternary diagram by C^0 and C^1 finite elements. Numerical experiments show the high efficiency of the new interpolation algorithm, which opens the way to its incorporation in a numerical flow simulator using the global pressure formulation. The compressibility factor $\partial P_c^g/\partial p(s,p)$ in the Darcy law for the global volumetric flow $\boldsymbol{q}$ as been shown to satisfy $0 \leqslant \partial P_c^g/\partial p \ll 1$ in the case of a single compressible phase. Further research will focus on how well TD-interpolation can match some experimental datas or a-priori given three-phase target permeability model such as [21] on the interior of $\mathbb{T}$. Two directions will be investigated:

- exploration of the class of TD-interpolation algorithms, in order to see how far one can match experimental or a-priori given three-phase target permeabilities such as [21],
- numerical comparison of the efficiency and precision of the conventional approach [21] with the exact global pressure formulation.

Acknowledgments

Financial support for this research from the Programme National de Recherche en Hydrologie (INSU-CNRS) and the Agence De l'Environnement et de la Maîtrise de l'Energie (ADEME) is gratefully acknowledged. The authors would also like to thank ADEME and Burgéap SA for financing the PhD scholarship of R. di Chiara Roupert.

References

[1] B. Amaziane, M. Jurak, A new formulation of immiscible compressible two-phase flow in porous media, C.R. Mécanique 336 (2008) 600–605.
[2] S.N. Antoncev, V.N. Monahov, Three-dimensional problems of time-dependent two-phase filtration in non-homogeneous anisotropic porous media, Soviet Math. Dokl. 19 (1978) 1354–1358.
[3] J. Argyris, I. Fried, D. Scharpf, The tuba family of plate elements for the matrix displacement method, J. Roy. Aeronaut. Soc. 72 (1968) 701–709.
[4] J. Bear, Dynamics of Fluids in Porous Media, Elsevier, New York, 1972.
[5] K. Bell, A refined triangular plate bending finite element, Int. J. Numer. Methods Eng. 1 (1969) 101–122.
[6] M. Bernadou, J.M. Boisserie, K. Hassan, Sur l'implémentation des éléments finis de Hsieh–Clough–Tocher complet et réduit, Inria Research Report RR-4, 1980.
[7] M. Bernadou, K. Hassan, Basis functions for general Hsieh–Clough–Tocher triangles complete or reduced, Inria Research Report RR-5, 1980.
[8] G. Chavent, A new formulation of diphasic incompressible flows in porous media, in: A. Dold, B. Eckman (Eds.), Applications of Methods of Functional Analysis to Problems in Mechanics, Lecture Notes in Mathematics, vol. 503, Springer, Berlin, 1976.
[9] G. Chavent, G. Salzano, Un algorithme pour la détermination de perméabilités relatives triphasiques satisfaisant une condition de différentielle totale, Inria Research Report RR-0355, 1985.
[10] G. Chavent, J. Jaffré, Mathematicals Models and Finite Elements of Reservoir Simulation, North-Holland, Amsterdam, 1986.
[11] G. Chavent, R. di Chiara Roupert, G. Schäfer, A fully equivalent global pressure formulation for three-phase compressible flows, in: Conference Scaling'Up 08, Dubrovnik, October 13–16, 2008.
[12] G. Chavent, A fully equivalent global pressure formulation for three-phase compressible flow, Appl. Anal. 88 (2009) 1527–1541.
[13] Z. Chen, R. Ewing, Comparison of various formulations of three-phase flows in porous media, J. Comput. Phys. 132 (1997) 362–373.
[14] Z. Chen, Finite Element Methods and Their Applications, Scientific Computation, Springer, Berlin, 2005.
[15] P. Ciarlet, The finite element method for elliptic problems, society for industrial and applied mathematics, J. Comput. Phys. 132 (1978) 362–373.
[16] R.W. Clough, J.L. Tocher, Finite element stiffness matrices for analysis of plate bending, in: Proceedings of the Conference on Matrix Methods in Structural Mechanics, Wright Patterson A.F.B., OH, 1965.
[17] T.A. Davis, I.S. Duff, A combined unifrontal/multifrontal method for unsymmetric sparse matrices, Technical Report TR-97-016, Computer and Information Science and Engineering Department, University of Florida, 1997.
[18] S.C. Eisenstat, Efficient implementation of a class of preconditioned conjugate gradient methods, SIAM J. Sci. Statist. Comput. 2 (1981) 1–4.

[19] S. Jégou, Estimation des perméabilités relatives dans des expériences de déplacements triphasiques en milieu poreux, Thése, Université Paris IX Dauphine, 1997.
[20] A. Quarteroni, R. Sacco, F. Saleri, Méthodes Numériques – Algorithme, analyse et applications, Springer, Italia, 2007.
[21] H.M. Stone, Probability model for estimating three-phase relative permeabilitiy, J. Petrol. Technol. 22 (1970) 214–218.